ELSEVIER

Journal of Hazardous Materials A139 (2007) 424–429

Journal of Hazardous Materials

www.elsevier.com/locate/jhazmat

Glass-ceramic materials from electric arc furnace dust

P. Kavouras, T. Kehagias *, I. Tsilika, G. Kaimakamis, K. Chrissafis, S. Kokkou, D. Papadopoulos, Th. Karakostas

Physics Department, Aristotle University of Thessaloniki, 54124 Thessaloniki, Greece

Available online 22 May 2006

Abstract

Electric arc furnace dust (EAFD) was vitrified with SiO_2, Na_2CO_3 and $CaCO_3$ powders in an electric furnace at ambient atmosphere. Vitreous products were transformed into glass-ceramic materials by two-stage heat treatment, at temperatures determined by differential thermal analysis. Both vitreous and glass-ceramic materials were chemically stable. Wollastonite ($CaSiO_3$) was separated from the parent matrix as the dominant crystalline phase, verified by X-ray diffraction analysis and energy dispersive spectrometry. Transmission electron microscopy revealed that wollastonite crystallizes mainly in its monoclinic form. Knoop microhardness was measured with the static indentation test method in all initial vitreous products and the microhardness values were in the region of 5.0–5.5 GPa. Devitrification resulted in glass-ceramic materials with microhardness values strongly dependent on the morphology and orientation of the separated crystal phase.

Keywords: Vitrification; Glass-ceramic; Wollastonite; Electron microscopy; Microhardness

1. Introduction

Electric arc furnace dust (EAFD) is a solid waste produced by the steel scrap recycling facilities, which represent a continuously growing portion of the global steel production. Namely, steel scrap recycling facilities fabricated 34% of the global steel production in 1998. EAFD has been recognized as the second largest continuously generated hazardous waste stream in the United States, while it is estimated that the world production will reach 5,000,000 t per year in 2005. In Greece, all five steel factories are scrap recycling facilities, where a total amount of 15,000 t of EAFD is produced annually. Such large quantities are justified from the fact that a total of 15–20 kg of EAFD is produced per ton of steel. EAFD contains significant quantities of lead in the form of lead oxide (PbO), iron and zinc compounds in the forms of zinc oxide (ZnO) and zinc ferrite ($ZnFe_2O_4$) and it is categorized as a hazardous solid waste according to the United States Environmental Protection Agency (USEPA) classification. It is created during melting of steel scrap in the electric arc furnaces, where heavy metals are volatilized, oxidized and subsequently solidified and detained in the form of fine powder, in specially designed filters, which are placed in the electric arc furnace gas stream cleaning system.

A part of metallic Zn is recovered from the EAFD by hydrometallurgical or pyrometallurgical processes. The resulting residue is a hazardous solid waste in powder form, since the above processes can recover only a part of the Zn content. It is thus essential to develop an additional process that stabilizes metallic Zn and the other heavy metals found in the residues of Zn recovery processes. One of the most promising methods is vitrification with the addition of batch materials [1]. Vitrification, except from a well established stabilization technique, poses as a method for the production of vitreous or glass-ceramic marketable materials that can be used for construction and decorative applications [2–6].

In this study, we present the results of the vitrification method on the stabilization of EAFD and the development of glass-ceramic materials. EAFD was initially mixed with $CaCO_3$, Na_2CO_3 and SiO_2 powders. The selection of the additional batch materials was based on the fact that they are found in abundance in some non-toxic wastes, e.g. in waste glass, marble dust, mussel shells or steel facility dust. In this way, the appropriate compositions that lead to the production of glass-ceramic materials can be subsequently simulated with the addition of the above-mentioned non-toxic wastes. By combining toxic and

* Corresponding author. Tel.: +30 231 0998023; fax: +30 231 0998589.
E-mail address: kehagias@auth.gr (T. Kehagias).

0304-3894/$ – see front matter © 2006 Elsevier B.V. All rights reserved.
doi:10.1016/j.jhazmat.2006.02.043

non-toxic solid wastes, for the production of marketable materials, vitrification can become an economically attractive method of solid waste management.

2. Experimental

EAFD powder was mixed with SiO_2, Na_2CO_3 and $CaCO_3$ powders in various proportions. The solid mixtures were placed in a Pt crucible and they were heated in an electric furnace at ambient atmosphere at 1400 °C for 2 h. The melt was poured on a stainless steel plate and was rapidly cooled down at room temperature. As-quenched products were pulverized and characterized by differential thermal analysis (DTA) in order to obtain the glass transition temperature (T_g) and the position of exothermic peaks that would presumably correspond to crystal phase separation. DTA scans were obtained with a Setaram TG-DTA SetSys 1750 °C instrument in argon atmosphere. Heating and cooling rates were set at 10 °C/min and the samples were placed in Al_2O_3 crucibles.

As-quenched products were subsequently heated at a temperature near T_g, namely 5 °C higher than T_g, for residual stress relaxation. These products will be referred to as initial products. A two-stage isothermal treatment process was applied to all initial products. In the first isothermal stage, nucleation takes place and in the second crystal growth occurs. The duration of these two stages was fixed at 15 min for the nucleation and 30 min for the crystal growth process. The nucleation stage was placed ≅200 °C below exothermic peaks maxima, while crystal growth stage was placed a few degrees above them.

All initial and annealed products were morphologically characterized by optical microscopy, using a Zeiss Axiolab-A microscope, scanning electron microscopy (SEM) with a JEOL JSM-840A microscope, equipped with an Oxford ISIS-300 energy dispersive spectrometry (EDS) analyzer. Structural characterization was performed by X-ray diffraction (XRD) analysis with a Seifert 3003 powder diffractometer, using Cu Kα1 radiation. Transmission electron microscopy (TEM) was employed for microstructural characterization. Specimens for TEM were thinned by mechanical grinding, followed by ion-thinning to reach electron transparency. TEM observations were carried out in a Jeol JEM-2011 electron microscope, operating at 200 kV.

The microhardness of initial and annealed products was measured with the static indentation method with Knoop indenter geometry, using an Anton-Paar MHT-10 microhardness tester, attached on a Zeiss Axiolab-A optical microscope. The indentation parameters were set at: load = 1 N, duration = 10 s and loading slope = 20 N/s. The loading slope was the smoothest obtainable from our tester in order to avoid cracking during indentation. The duration of 10 s is a typical time that is long enough for the onset of plasticity. In order to resolve the indentation load that would be used for measurements, the indentation size effect (ISE) curves were obtained for all samples. The load of 1 N was found to lie in the plateau region of the ISE curve in all samples and was low enough to avoid microcrack propagation. The microhardness values represent the mean value of 12 crackless [7] indentations.

3. Results

3.1. EAFD composition

A mass of 1 kg of EAFD was mechanically homogenized and refined with a vibrating frame ball milling apparatus. The resulting powder was used to form 10 green state disk shaped compacts of 3 cm in diameter. Their elemental composition was determined by EDS and the structural analysis was performed by XRD. Additionally, EAFD powder was heated up to 1000 °C to determine the loss on ignition (LOI) mass. EAFD composition is shown in Table 1. The two main constitutive oxides are iron oxide and zinc oxide, in accordance with other researchers [8]. The corresponding XRD diagram is presented in Fig. 1, where the high intensity peaks correspond to $ZnFe_2O_4$ (zinc ferrite) and ZnO. Some low intensity peaks correspond to PbO.

3.2. Vitrification process

Batch compositions are listed in Table 2. As-quenched products were subjected to stress relief at temperatures 5 °C higher than T_g (Table 2) that was obtained by DTA scans, presented in Fig. 2. The resulting stress relieved initial products were X-ray amorphous, as it was confirmed by XRD analysis (Fig. 3). EDS analyses showed that all elements were homogeneously

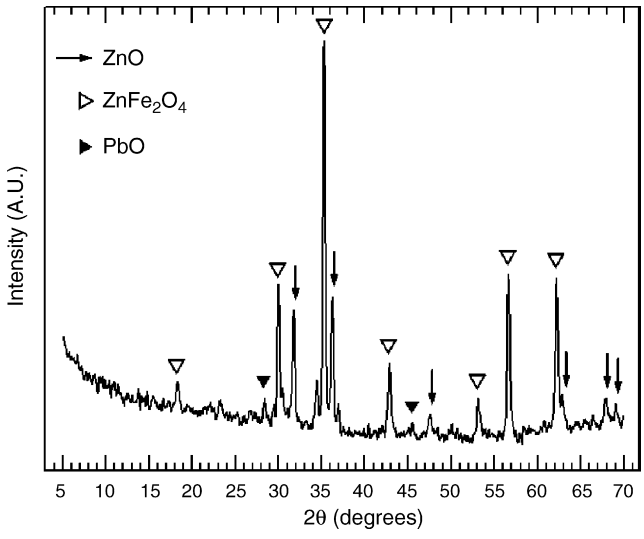

Fig. 1. X-ray diffractogram of the pulverized and homogenized EAFD waste.

Table 1
Composition of EAFD powder in oxide compounds

Compound	MgO	Al_2O_3	SiO_2	K_2O	CaO	MnO	Fe_2O_3	ZnO	PbO	LOI	Humidity
Composition (wt%)	0.7	0.9	4.1	1.4	4.6	3.3	33.9	34.9	6.2	7.8	2.0

Table 2
Batch compositions (wt%), glass transition temperatures (T_g) and temperature intervals between exothermic peak maxima (T_{max}) and the corresponding glass transition temperatures obtained from DTA scans

	SiO_2	Na_2O	CaO	EAFD	T_g (°C)	T_{max}–T_g (°C)	Si/O
EAFD1	55	10	15	20	584	322	0.360
EAFD2	55	5	20	20	631	277	0.359

The silicon over oxygen (Si/O) atomic ratio is also presented.

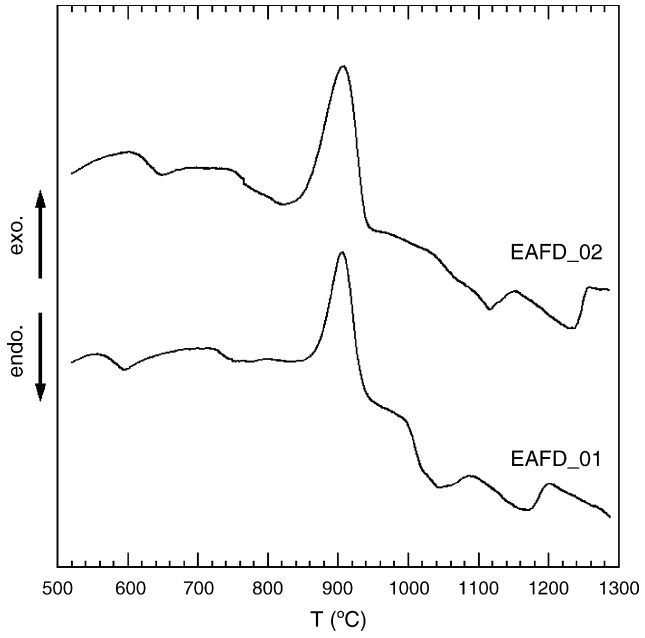

Fig. 2. DTA thermographs of the two initial vitrified products.

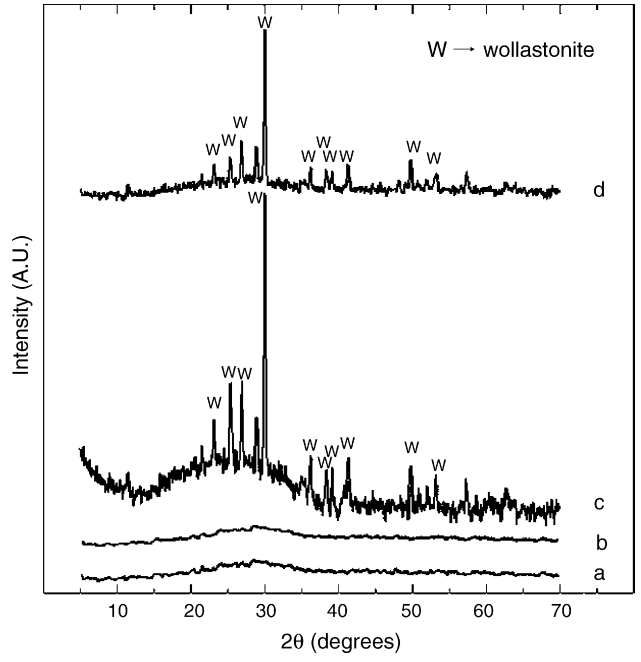

Fig. 3. X-ray diffractograms of the initial EAFD1 and EAFD2 products (a and b) and thermally treated products EAFD1 and EAFD2 (c and d).

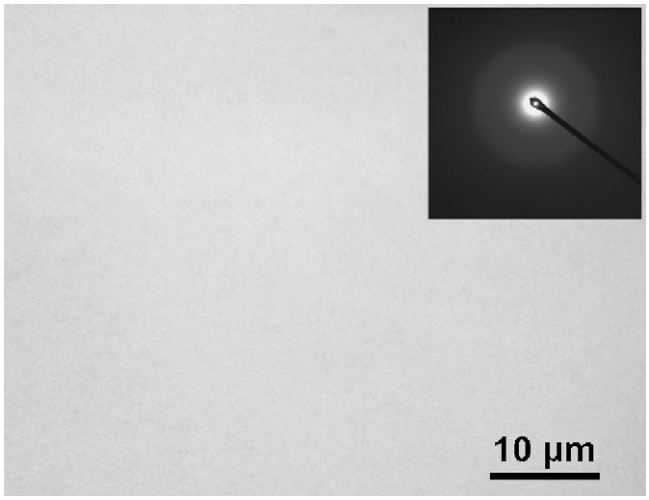

Fig. 4. Bright field (BF) TEM micrograph of the amorphous matrix of EAFD1 initial product. The corresponding ED pattern is shown as an inset.

dispersed through the vitreous matrix, since the standard deviations of elemental compositions did not exceed ±1% that is the minimum standard deviation of the EDS method.

TEM observations confirmed that both initial products were amorphous. Electron diffraction (ED) patterns obtained from initial products were composed of a diffused halo around the transmitted spot, indicative of an amorphous structure. A characteristic TEM micrograph of EAFD1 initial product and the corresponding ED pattern are shown in Fig. 4.

3.3. Thermally treated products

Thermal treatment of the initial products was performed in two stages at temperatures determined from the DTA scans: nucleation temperature (T_n) at 680 °C for 15 min and crystal growth temperature (T_{gr}) at 900 °C for 30 min. Thermally induced transformations were initially inspected by optical microscopy on mechanically polished cross-sections. In the case of thermal treatment of EAFD1 composition, it was found that crystal growth occurred in the form of needle-like crystallites emanating from the surface of the samples. The crystallites were wollastonite needles, as it was verified by XRD analysis (Fig. 3). Fig. 5a is an optical micrograph of a polished section of thermally treated EAFD1 composition observed under reflected light.

Fig. 5b is an optical micrograph from a characteristic region of a thermally treated EAFD2 product, observed under reflected light. In this case, the morphology of the separated crystalline phase is different: thermal treatment resulted in an isotropic glass-ceramic material, i.e. a product with homogeneously dispersed crystallites that XRD analysis identified also as wollastonite phase (Fig. 3). The size (d) of wollastonite crystallites varies in the range of $2 \leq d \leq 8$ μm. TEM observations confirmed the existence of wollastonite as the dominant crystalline phase in both devitrified samples. Fig. 6 is a bright-field (BF) TEM micrograph depicting a needle-like wollastonite crystallite of monoclinic symmetry, as it is revealed from the corresponding ED patterns. However, triclinic wollastonite was also detected, much less frequently though.

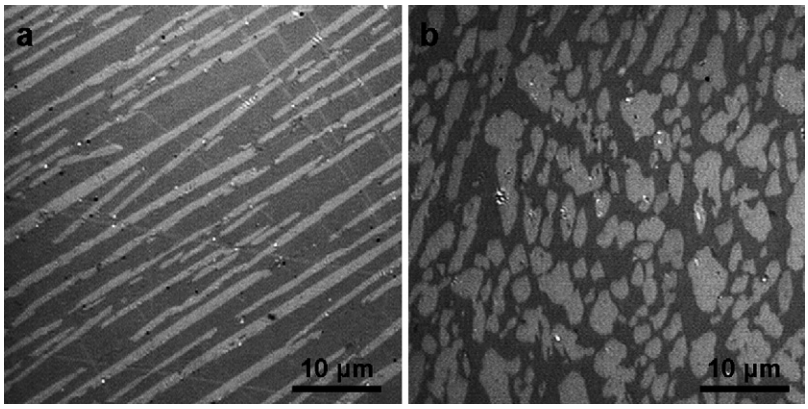

Fig. 5. Optical micrographs from: (a) EAFD1 and (b) EAFD2 annealed samples observed under reflected illumination.

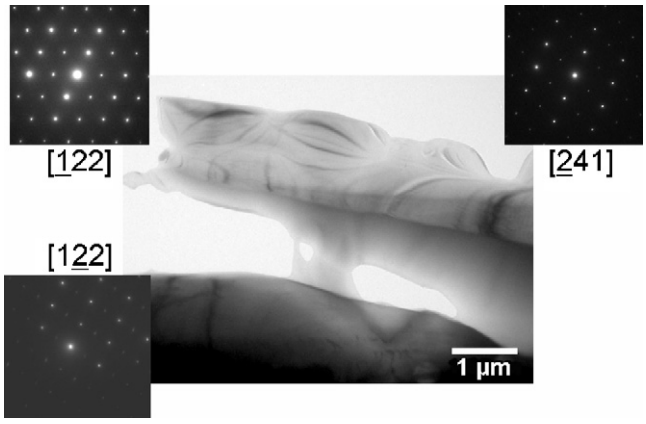

Fig. 6. BF TEM micrograph of a needle-like wollastonite crystallite that grew inside the residual matrix of heat-treated EAFD1 product. The ED patterns were obtained from the same crystallite depicted in the BF image.

3.4. Microhardness characterization

The microhardness of all starting and annealed products was characterized by the static indentation method utilizing a Knoop diamond indenter. As it was mentioned in Section 2, all microhardness measurements were made with the same indentation load, namely 1 N that lies in the plateau region of the ISE effect for all specimens. As a result, all measurements can be safely compared in a quantitative manner. The results are listed in Table 3. The microhardness value of EAFD2 initial product is roughly the same compared to EAFD1. In the case of

Table 3
Microhardness test results

Product	Treatment	H_K (GPa)
EAFD1	Starting	5.38 ± 0.13
EAFD1	Annealed, H_K(a)	5.25 ± 0.08
EAFD1	Annealed, $H_K(\perp)$	4.91 ± 0.19
EAFD1	Annealed, $H_K(\|\|)$	4.23 ± 0.14
EAFD2	Starting	5.58 ± 0.07
EAFD2	Annealed	6.04 ± 0.15

The errors represent the standard deviations.

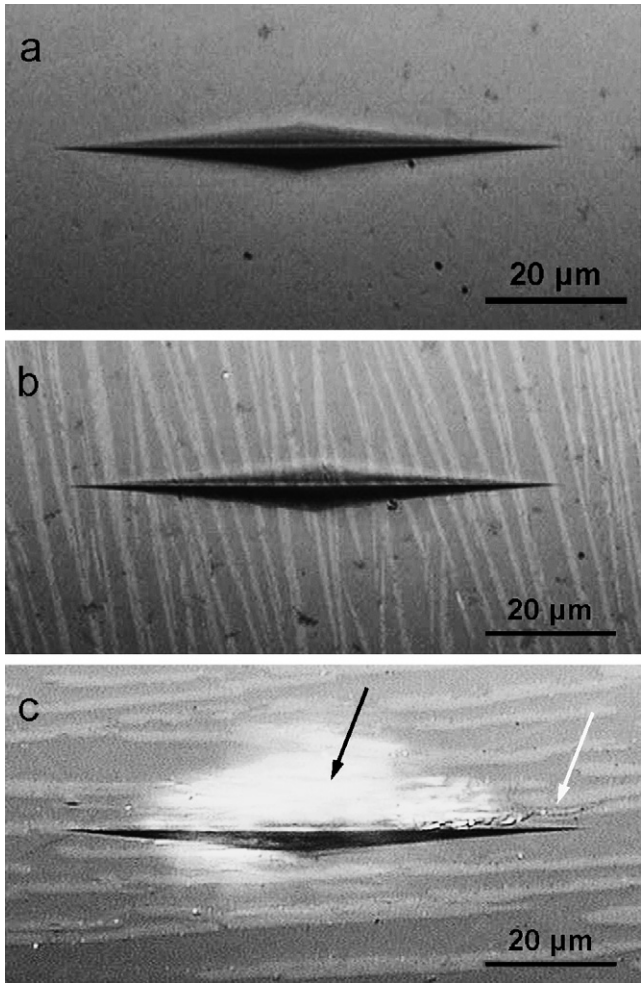

Fig. 7. Characteristic optical micrographs of Knoop indentation prints from EAFD1 products (a) inner amorphous core, (b) vertically and (c) parallel positioned indentation prints, with respect to the needle-like wollastonite crystallites in an annealed product. The white arrow indicates a microcrack that propagated along the interface of a needle-like crystallite and the residual matrix. The black arrow indicates a bright halo that comes from the reflectance of incident light from newly created surfaces below the surface.

annealed EAFD1 product, three distinct microhardness values were obtained: one from the inner non-devitrified volume and two from the devitrified zone. The microhardness value from the non-devitrified volume (H_K(a)) is virtually not affected from thermal treatment. In the devitrified zone, two series of measurements were performed: one with the large Knoop indenter diagonal perpendicular ($H_K(\perp)$) and one parallel ($H_K(||)$) to the needle-like crystallites. In the former case, the microhardness value was found to be higher with respect to the latter, while both microhardness values were lower compared to the initial vitreous product. Knoop indentations with the same load on the amorphous and devitrified regions are depicted in Fig. 7. It was also observed that microcracks showed preferential propagation in directions parallel to the needle-like crystallites (Fig. 7c). Thermal treatment of EAFD2 initial product resulted in a glass-ceramic material with higher microhardness value by ≅0.5 GPa.

4. Discussion

Initial and thermally treated products successfully incorporate zinc, iron and lead oxides. This was verified from the fact that all products remained in pristine state after the influence of strong acidic conditions. All samples remained virtually intact after 1 week in HCl solution of 37% (w/w). This can be explained from the concentration of SiO_2 in the batch materials, which is the main glass former. The silicon over oxygen atomic ratio (Si/O) is higher than 0.33 in both initial materials (Table 2). For such high values of Si/O, silica is able to construct an extended three-dimensional vitreous network with the desired structural integrity [9]. It is also important that the initial products were compositionally homogeneous, i.e. the composition was not in the region of a stable or meta-stable immiscibility gap that would result in undesirable inhomogeneity, which could deteriorate the chemical resistance [2]. Consequently, both batch compositions could be used for the production of stabilized vitreous products. However, they have different behavior to devitrification.

EAFD1 is less receptive to devitrification than EAFD2. This can be established by comparing the XRD diagrams c and d in Fig. 3. XRD diagram c contains a characteristic amorphous bump, while it is absent in diffractogram d. This results from the higher intensity of the wollastonite peaks that render the intensity of the amorphous hump negligible, in the case of devitrified EAFD2 product. This observation is in accordance with the wider temperature interval between the maximum of the exothermic peak that corresponds to the crystallization peak and the glass transition found in EAFD1, compared to EAFD2 (Table 2). It is well established that a vitreous material with wider temperature interval presents higher thermal stability than another one with narrower temperature interval [10]. As a result, EAFD2 can be transformed into a glass-ceramic material in less time, with evident benefits in terms of cost-effectiveness.

The fact that EAFD1 is less receptive to devitrification may be due to the different relative proportion of the two modifying oxides (Na_2O and CaO) that can be interpreted by the concept of mixed modifier effect (MME), an effect similar to the well known mixed alkali effect (MAE) [12]. MAE is a phenomenon that affects all properties of glasses, which strongly depend on long-range motion of ions, by deviating from simple additive behavior upon mixing of two different types of mobile ions [13]. MME has been used to interpret the durability of nuclear waste glasses [14]. More specifically, wollastonite separation is based on reconstructive transformation, i.e. transformation that requires long-range diffusion of the crystal phase components, since the initial glass matrix has a different composition than wollastonite. Thus, it is reasonable to expect higher tendency of wollastonite separation to EAFD2 thermally treated product, since in that case the Na^+/Ca^{2+} atomic ratio is 0.45, while in the case of EAFD1 is 0.90.

Another important parameter that evidences EAFD2 thermally treated product to be more useful is the difference in the morphology of separated wollastonite crystallites. Two-stage thermal treatment of EAFD1 produced a material with a devitrified surface zone, where the needle-like wollastonite crystallites were oriented normally to the surface. Nucleation time did not have any observable influence on the extent of devitrification, while longer crystal growth times resulted to wider devitrified zones that grew at the expense of the central amorphous region. Contrarily, thermal treatment of EAFD2, with the same conditions, resulted to a material that consisted of a residual amorphous matrix with homogeneously dispersed wollastonite crystallites of a few micrometers in size. According to the widely accepted definition by Strnad [11], only devitrified EAFD2 can be considered as a glass-ceramic material. Additionally, the difference in wollastonite morphology has important consequences on the microhardness and crack propagation patterns.

Mechanical properties were studied, in order to determine the application areas of the glass-ceramic product that is produced from the stabilization of solid wastes. Microhardness is a basic parameter in order to decide whether a product can be used or not for construction applications [15]. The microhardness values of EAFD1 and EAFD2 initial products are roughly the same. This is due to the fact that the difference in the composition between the two products was achieved by the mutual exchange of Na_2O for CaO, both being modifying oxides. As a result, the depolymerization of the vitreous network was not appreciably affected. Consequently, the activation of densification and plastic flow [16], being the two basic mechanisms for plastic deformation were not altered, since they are based on the rupture of atomic bonds [17].

The microhardness value of the central non-devitrified region of EAFD1 thermally treated product had the same microhardness value, within the experimental errors. This is due to the fact that this region had roughly the same composition as the initial product. The microhardness value was found to be depending on the orientation of the Knoop indentation print with respect to the orientation of the needle-like crystallites. These crystallites acted as a barrier to plastic flow, hindering plastic deformation, which resulted to higher $H_K(\perp)$ value compared with the $H_K(||)$ value. Additionally, indentation parallel to the needle-like crystallites produced surface microcracks that propagated parallel to them, in the load regime where crackless indentation prints were obtained for the normal orientation of the Knoop indenter. Apparently, microcracks could not penetrate the wollastonite crystallites and they were deflected from the

matrix/crystallite interface. This originates from the weaker adhesion of the crystallite-residual vitreous matrix that renders the propagation of microcracks along the interface energetically favorable. Similar behavior has been observed in many fibre reinforced composite materials and it is known as interfacial debonding [18]. This is another possible reason that $H_K(\perp)$ is higher compared to the $H_K(||)$ value [19]. Additionally, new free surfaces have been created in the interior of the sample, possibly freshly debonded crystallites due to microcracks that propagated normally to the surface [20]. The new free surfaces reflected the incident light and formed the bright halo around the Knoop indentation (Fig. 7c, black arrow).

EAFD2 devitrified product has a higher microhardness value by 0.5 GPa, compared with its initial vitreous product. This is a common phenomenon that has also been observed in other cases [21] and it was induced from the homogeneously dispersed wollastonite crystallites that acted as a second phase hindering plastic flow. Additionally, there was not any orientation found for preferential microcrack propagation. This is another effect of the isotropic character of nucleation. Consequently, EAFD2 devitrified product is a material that can be potentially utilized for construction applications. This is due to a number of attractive physical characteristics, like chemical stability, isotropic crystal phase separation, microhardness and lack of preferential microcrack propagation direction.

5. Conclusions

EAFD powder was mixed with SiO_2, Na_2CO_3 and $CaCO_3$ powders and two different batch compositions were prepared for the production of vitreous products. In all cases, wollastonite was separated as the dominant crystalline phase after thermal treatment. Initial vitreous and glass-ceramic products, successfully immobilized Zn and Pb, which are the main hazardous elements found in EAFD. This was found by the negligible weight loss after the exposure of all products in strong acidic conditions for several days. EAFD2 batch composition was found to be the most appropriate for large-scale stabilization of EAFD. It was more receptive to devitrification and the separated wollastonite crystallites were homogeneously distributed over the whole volume of the sample and had similar sizes. The isotropic character of nucleation led to a material with higher microhardness value with respect to the parent vitreous product and without preferential microcrack propagation direction.

Acknowledgements

This work was co-funded by the European Social Fund and National resources through the EPEAEK II “Pythagoras” program.

References

[1] J.R. Conner, S.L. Hoeffner, A critical review of stabilization/solidification technology, Crit. Rev. Environ. Sci. Technol. 28 (1998) 397–462.
[2] P. Kavouras, G. Kaimakamis, T.A. Ioannidis, T. Kehagias, P. Komninou, S. Kokkou, E. Pavlidou, J. Antonopoulos, M. Sofoniou, A. Zouboulis, C.P. Hadjiantoniou, A. Prakouras, T. Karakostas, Vitrification of lead-rich solid ashes from incineration of hazardous industrial wastes, Waste Eng. 23 (2003) 361–371.
[3] M. Romero, R.D. Rawlings, J.M. Rincón, Development of new glass-ceramic by means of controlled vitrification and crystallization of inorganic wastes from urban incineration, J. Eur. Ceram. Soc. 19 (1999) 2049–2058.
[4] E. Haugsten, B. Gustavson, Environmental properties of vitrified fly ash from hazardous and municipal waste incineration, Waste Manage. 20 (2000) 167–176.
[5] L. Barbieri, A. Corradi, I. Lancellotti, Alkaline and alkaline-earth silicate glasses and glass-ceramics from municipal and industrial wastes, J. Eur. Ceram. Soc. 20 (2000) 2477–2483.
[6] J. Sheng, Vitrification of borate waste from nuclear power plant using coal fly ash. (II) Leaching behaviour of the FA30 glass, Fuel 81 (2002) 253–256.
[7] L. Hong, R.C. Bradt, The effect of indentation-induced cracking on the apparent microhardness, J. Mater. Sci. 31 (1996) 1065–1070.
[8] T. Solifić, A. Rastovčan-Mioč, Š. Cerjan-Stefanović, V. Novosel-Radović, M. Jenko, Characterization of steel mill electric-arc furnace dust, J. Hazard. Mater. B109 (2004) 59–70.
[9] J.E. Shelby, Introduction to Glass Science and Technology, RSC Paperbacks, Cambridge, 1997.
[10] A. Hrubý, Evaluation of glass-forming tendency by means of DTA, Czech. J. Phys. B22 (1972) 1187.
[11] Z. Strnad, Glass-Ceramic Materials, Elsevier, Amsterdam, 1986.
[12] J. Zarzycki, Glasses and the Vitreous State, Cambridge University Press, 1990.
[13] D. Day, Mixed alkali glasses—their properties and uses, J. Non-Cryst. Solids 21 (1976) 343–372.
[14] S.V. Raman, The effect of mixed modifiers on nuclear waste glass processing, leaching and Raman spectra, J. Mater. Res. 13 (1998) 8–15.
[15] M. Erol, S. Küçükbayrak, A. Ersoy-Meriçboyu, M.L. Överçoğlu, Crystallization behaviour of glasses produced from fly ash, J. Eur. Ceram. Soc. 21 (2001) 2835–2841.
[16] R.H. Doremus, Glass Science and Technology, John Wiley and Sons, New York, 1994.
[17] S.N. Salama, H.A. El-Batal, Microhardness of phosphate glasses, J. Non-Cryst. Solids 168 (1994) 179–185.
[18] D. Hull, T.W. Clyne, An Introduction to Composite Materials, Cambridge University Press, 1996.
[19] H. Li, R.C. Bradt, The effect of indentation-induced cracking on the apparent microhardness, J. Mater. Res. 31 (1996) 1065–1070.
[20] R.F. Cook, G.M. Pharr, Direct observation and analysis of indentation cracking in glasses and ceramics, J. Amer. Ceram. Soc. 73 (1990) 787–817.
[21] P. Kavouras, P. Komninou, T. Karakostas, Effect of composition and annealing temperature on the mechanical properties of a vitrified waste, J. Eur. Ceram. Soc. 24 (2004) 2095–2102.